Mobility in semiconducting graphene nanoribbons: Phonon, impurity, and edge roughness scattering

Tian Fang, Aniruddha Konar, Huili Xing, and Debdeep Jena[*]

Department of Electrical Engineering, University of Notre Dame, Notre Dame, Indiana 46556, USA
(Received 1 July 2008; revised manuscript received 17 September 2008; published 4 November 2008)

The transport properties of carriers in semiconducting graphene nanoribbons are studied by comparing the effects of phonon, impurity, and line-edge roughness scattering. It is found that scattering from impurities located at the surface of nanoribbons and from acoustic phonons are as important as line-edge roughness scattering. The relative importance of these scattering mechanisms varies with the temperature, Fermi-level location, and the width of the ribbons. Based on the analysis, strategies for improvement of low-field mobility are described.

I. INTRODUCTION

Since the isolation of two-dimensional (2D) graphene sheets in 2004,[1–3] there has been substantial interest in patterning them into quasi-one-dimensional (quasi-1D) graphene nanoribbons (GNRs).[4] The ability to tune the energy gaps of GNRs lithographically will facilitate lateral band-gap-engineered electronic devices. GNRs as thin as ~ 3 nm have been achieved, exhibiting band gaps approaching 0.3–0.4 eV, which makes them attractive for many low-power device applications.[5,6] The measured carrier mobilities in the first ultrathin GNRs are reported to be much lower[7] than in corresponding 2D graphene sheets.[8] Carrier transport properties and scattering mechanisms in 2D sheets of graphene have received a lot of attention recently, and a coherent picture is emerging.[9–13] However, transport in GNRs has not received as much attention. For improvements in the transport properties of GNRs, it is essential to identify the major sources of carrier scattering. To that end, this work presents a comprehensive analysis of various scattering mechanisms that affect carrier mobilities in GNRs. Analytical scattering rates for phonon, impurity, and line-edge roughness (LER) scattering are derived taking the GNR wave functions into account. It is shown that carrier mobilities in GNRs are not necessarily limited by edge roughness scattering; similar to the case in 2D graphene, surface impurity[14] and phonon scattering play important roles depending on the carrier concentrations, widths, and temperature. The results of this work are expected to provide useful strategies toward improvements in carrier transport properties in GNRs for various applications.

The paper is structured in the following fashion. Section II describes the theoretical formalism used for the scattering rate and mobility calculations, with a discussion of the electronic structure, scattering matrix elements, and screening in GNRs. In Sec. III, individual scattering rates due to acoustic and optical phonons, LER, and bulk and surface impurities are derived. Finally, in Sec. IV, the resulting mobility in GNRs is calculated, with a discussion of the relative importance of the various scattering mechanisms. The effect of temperature, location of Fermi level, and GNR width on the transport properties is evaluated in that section.

II. THEORETICAL FORMALISM

Under the application of a small electric field along the GNR axis, the carrier distribution function in the relaxation-time approximation is given by[15]

$$f \approx f_0 - (e\tau v_g \mathcal{F})\left(-\frac{\partial f_0}{\partial \mathcal{E}}\right), \tag{1}$$

where τ^{-1} is the scattering rate in the diffusive limit, v_g is the group velocity of carriers, $\mathcal{F}$ is the electric field, e is the electron charge, $\mathcal{E}$ is the energy, and f_0 is the equilibrium Fermi-Dirac distribution. If the scattering rate is known, the current flowing through the GNR may be evaluated by the relation,

$$I = e(g_s g_v/L)\sum_k f v_g, \tag{2}$$

where e is the electron charge, L is the GNR length, $g_s = 2$ is the spin degeneracy, and $g_v = 1$ is the valley degeneracy of semiconducting GNRs. Noting that the electric field is $\mathcal{F} = V/L$, where V is the applied voltage, the 1D conductivity (in units of S m) is given by

$$\sigma_{1D} = \frac{4e^2}{h}\int_0^\infty v_g(\mathcal{E})\tau(\mathcal{E})\left(-\frac{\partial f_0}{\partial \mathcal{E}}\right)d\mathcal{E}, \tag{3}$$

where $h = 2\pi\hbar$ is the Planck constant. The mobility is calculated as $\mu = \sigma_{1D}/en_{1D}$, where n_{1D} is the one-dimensional carrier density. This formalism allows for the evaluation of scattering rates, mobility, and conductivity for a general Fermi-level location, which can be assumed to be tuned capacitively through a gate voltage in experiments, at any temperature. To evaluate the conductivity and the resulting mobility, the group velocity and the scattering rates are required. Since they are related to the electronic band structure of the material, a brief discussion of the electronic band structure is given next.

A. Electronic structure

Semiconducting armchair GNRs with lengths $L(\gg W)$ along the y (x) directions are considered in this work. The hard-wall boundary conditions at the edges lead to a band

structure $\mathcal{E}(k_n, k_y) = \hbar v_F \sqrt{k_n^2 + k_y^2}$, where $v_F \sim 10^8$ cm/s is the Fermi velocity.[16,17] The allowed transverse wave vector for semiconducting armchair GNRs are quantized to values $k_n = \pm n\pi/3W$, depending on the width W; here $n = \pm 1, \pm 2, \pm 4, \pm 5, \pm 7, \pm 8, \ldots$ The resulting band gap is $\mathcal{E}_g = 2\pi \hbar v_F / 3W$, which is $\sim 1.38/W$ eV, with W expressed in nanometer.[16] We note that the group velocity of carriers in a GNR is linked to the density of states (DOS) ρ_{GNR} by $v_g(\mathcal{E}) = 2/\pi \hbar \rho_{\mathrm{GNR}}(\mathcal{E})$, where the DOS is $\rho_{\mathrm{GNR}}(\mathcal{E}) = (2/\pi \hbar v_F) \times [\mathcal{E}/\sqrt{\mathcal{E}^2 - (\mathcal{E}_g/2)^2}]$ for the first subband. The effective 1D carrier density in the GNR is given by $n_{\mathrm{1D}} = \int_0^\infty \rho_{\mathrm{GNR}}(\mathcal{E}) f_0(\mathcal{E}) d\mathcal{E}$. With this form of group velocity and carrier concentration, the only remaining undetermined quantities for evaluating mobility are the energy-dependent scattering rates. The procedure for finding the scattering rates is described next.

B. Matrix elements and scattering rates

Since the scattering rates depend on the nature of the scattering potential, we first discuss the formalism for the scattering rates for a general potential, and then consider specific scattering events. Scattering rates are evaluated using Fermi's golden rule, which requires the wave functions of the carriers, and matrix elements of the form $\langle f|V|i\rangle$, where $|i\rangle, |f\rangle$ are the initial and final states and V the scattering potential, which is a perturbation to the perfect crystalline periodic potential. We first discuss the real-space representation of the wave functions and outline a general procedure for calculating scattering rates. Then, we consider each scattering mechanism separately by modeling them with representative potentials.

The electronic wave functions of carriers in semiconducting GNRs may be derived from an admixture of states in the $\mathcal{K}$ and $\mathcal{K}'$ valleys of the underlying 2D graphene band structure.[17] For armchair semiconducting GNRs, the valley degeneracy is removed. Assuming a length L and a width W, the electronic wave functions in the nth subband in the Ket notation are written as

$$|\varphi\rangle = \frac{1}{\sqrt{2}}|k_n, k_y\rangle - \frac{1}{\sqrt{2}}|\widetilde{k_n}, k_y\rangle, \tag{4}$$

where the tilde sign indicates the state in the $\mathcal{K}'$ valley. The resulting energy dispersion (the $\mathcal{E}$-k relation) of the nth subband is $\mathcal{E}(k_n, k_y) = \hbar v_F \sqrt{k_n^2 + k_y^2}$, where $v_F \sim 10^8$ cm/s is the Fermi velocity in graphene. The projections of these states on the real space give the wave functions,

$$\langle \mathbf{r}|k_n, k_y\rangle = \sqrt{\frac{1}{2LW}} e^{ik_y y} e^{i[(\Delta K/2 - k_n)]x} \begin{pmatrix} 1 \\ -e^{i\theta_n} \end{pmatrix},$$

$$\langle \mathbf{r}|\widetilde{k_n}, k_y\rangle = \sqrt{\frac{1}{2LW}} e^{ik_y y} e^{i[(k_n - \Delta K/2)]x} \begin{pmatrix} 1 \\ -e^{i\theta_n} \end{pmatrix}, \tag{5}$$

where $\mathbf{r} = (x, y)$ is the vector in the x-y plane. The two-component "spinor" nature of the wave functions result from the underlying graphene Dirac Hamiltonian, as has been described in Refs. 16 and 17. $\Delta K = 4\pi/3a$ is the distance be-

tween two Dirac points in the k space for the underlying 2D graphene band structure, a being the lattice constant of graphene. $\frac{\Delta K}{2} - k_n$ is the electron wave vector in the confined x direction for the nth subband states. θ_n is the angle between k_y and k_n, $\theta_n = \tan^{-1}(k_y/k_n)$. Since the carrier states in the k space are close to the Dirac point, $k_n \ll \Delta K$.

Carriers scatter due to electronic potentials that deviate from perfect crystallinity—these potentials could be caused by impurities, defects, or phonons. For a general perturbation potential of the form $V(x, y, z)$, the perturbation matrix element is given by

$$\langle \varphi'|V(x,y,z)|\varphi\rangle = \frac{1}{2}\{\langle k_y', k_{n'}|V|k_n, k_y\rangle + \langle \widetilde{k_y'}, \widetilde{k_{n'}}|V|\widetilde{k_n}, k_y\rangle\}$$
$$- \frac{1}{2}\{\langle k_y', \widetilde{k_{n'}}|V|k_n, k_y\rangle + \langle k_y', k_{n'}|V|\widetilde{k_n}, k_y\rangle\}. \tag{6}$$

For finding the mobility and conductance, the scattering rates due to various scattering mechanisms are evaluated using Fermi's golden rule, in the form,

$$S(\mathbf{k}, \mathbf{k}') = \frac{2\pi}{\hbar}|\langle \varphi'|V(x,y,z)|\varphi\rangle|^2 \delta(\mathcal{E}_{\mathbf{k}} - \mathcal{E}_{\mathbf{k}}' \pm \hbar\omega), \tag{7}$$

where the delta function ensures energy conservation for both elastic ($\omega = 0$) and inelastic ($\omega \neq 0$) scattering processes. The ensemble scattering rate that contributes to the conductivity and mobility is then evaluated for each scattering mechanism as

$$\frac{1}{\tau} = \sum_k S(\mathbf{k}, \mathbf{k}')(1 - \cos \alpha), \tag{8}$$

α is the angle between $\mathbf{k}$ and $\mathbf{k}'$ and the summation runs over all available final states.

C. Screening

Screening of the scattering potential by free carriers in the GNRs modifies the scattering rates. To take this many-body effect into account, the following procedure has been used (see Ref. 18). The static screening is calculated using the random-phase approximation (RPA). In the k space, the relation between screened potential and unscreened potential is determined by $V^{\mathrm{uns}}(q_n, q_y) = \Sigma_m \epsilon(q_m, q_n, q_y) V^{\mathrm{scr}}(q_m, q_y)$. The screening matrix is given by

$$\epsilon(q_m, q_n, q_y) = \delta_{q_m q_n} + \frac{e^2}{2\pi \epsilon_0 \kappa} \mathcal{F}(q_m, q_n, q_y) \mathcal{L}(q_n, q_y), \tag{9}$$

where ϵ_0 is the permittivity of vacuum, κ is the average of the dielectric constants of the regions between which the GNR is sandwiched, and $\delta_{q_m q_n}$ is the Kronecker sign. $\mathcal{F}(\ )$ is a measure of the contribution to screening from coupled transverse modes given by

$$\mathcal{F}(q_m, q_n, q_y) = \frac{1}{2W^2} \int_0^W \int_0^W K_0(|q_y(x - x')|)$$
$$\times \cos(q_m x)\cos(q_n x')dxdx', \qquad (10)$$

where $K_0(\ldots)$ is the zero-order modified Bessel function. $\mathcal{L}(q_n, q_y)$ is given by

$$\mathcal{L}(q_n, q_y) = \sum_{|\delta k_{nn'}| = q_n} \mathcal{L}_{nn'}(q_y), \qquad (11)$$

which is a sum over Lindhard functions $\mathcal{L}_{nn'}$ between two subbands that have a wave-vector difference q_n in the transverse (x direction). This sum includes both intersubband and interband (conduction and valence band) contributions. The Lindhard function is given by

$$\mathcal{L}_{nn'}(q_y) = \frac{g_s}{L} \sum_{k_y} (1 + ss' \cos \theta_{kk'}) \frac{f_n(k_y) - f_{n'}(k_y + q_y)}{\mathcal{E}_{\mathbf{k}'} - \mathcal{E}_{\mathbf{k}}}, \qquad (12)$$

where $s = 1$ is for conduction subbands, $s' = -1$ is for valence subbands, $g_s = 2$ is the spin degeneracy, and $f_n(\ldots)$ is the Fermi-Dirac distribution function in the nth subband. If $|q_m - q_n| = l\pi/W$ and l is an odd number, $\mathcal{F}(q_m, q_n, q_y) = 0$. This makes the screening calculation very simple for the lowest subbands. The screening of the first subband is $\epsilon_{\mathrm{scr}} = \epsilon(0, 0, q_y)$, which is given by

$$\epsilon_{\mathrm{scr}} = 1 + \frac{e^2}{2\pi\epsilon_0\kappa} \mathcal{F}(0, 0, q_y)\mathcal{L}(0, q_y), \qquad (13)$$

which is equal to 1 if screening is neglected. In the long-wavelength limit ($q_y \to 0$), this evaluates to $\epsilon_{\mathrm{scr}} \approx 1 + (e^2/2\pi\epsilon_0\kappa) \times \rho_{\mathrm{GNR}}(\mathcal{E}_F)\ln(2/q_y W)$, whereas in the metallic limit ($q_y W \gg 1$), it is given by $\epsilon_{\mathrm{scr}} \approx 1 + e^2/\pi^2\epsilon_0\kappa\hbar v_F$. The general form given in Eq. (13) is used for the calculations that follow.

III. SCATTERING MECHANISMS

Low-field carrier transport in GNRs is affected by various scattering mechanisms. Among them, scattering by acoustic and optical phonons, charged impurities, and edge roughness scattering are expected to be most effective (see, for example, Refs. 19 and 20). Other mechanisms such as remote optical phonons due to polar coupling with underlying substrates or dielectrics may be present but are not considered in this work. Among the scattering mechanisms considered, phonon scattering sets the intrinsic limit on carrier mobilities. For GNRs with imperfect edges, LER scattering can be rather strong for very thin ribbons. Unintentional charged impurities present either attached to the GNRs or spatially separated from them (for example, embedded in the dielectric surrounding) also degrade the mobility. These scattering mechanisms (acoustic and optical phonons, LER, and charged impurity scattering) are considered in this work; their effects are compared, and their relative importance is qualitatively and quantitatively evaluated.

A. Acoustic phonons

For acoustic-phonon scattering, the zone-center acoustic-phonon interaction with carriers result in intravalley scattering, which is quasielastic. Here we only consider the longitudinal mode since this mode induces higher deformation potential than the out-of-plane and flexural modes.[21] The perturbation potential introduced by acoustic phonons is given by[22]

$$V_{\mathrm{ac}}(y) = \sqrt{\frac{n^{\pm}\hbar}{2\rho LW\omega_{\mathrm{ac}}}} D_{\mathrm{ac}} q_y e^{iq_y y}, \qquad (14)$$

where $n^- = 1/[\exp(\hbar\omega_{\mathrm{ac}}/k_B T) - 1]$, $n^+ = 1 + n^-$, $\omega_{\mathrm{ac}} = v_s q_y$ is the acoustic-phonon frequency, $D_{\mathrm{ac}} \sim 16$ eV is the deformation potential of acoustic phonons,[23] $\rho \sim 7.6 \times 10^{-8}$ g/cm^2 is the 2D mass density of graphene, and $v_s \sim 2 \times 10^6$ cm/s is the sound velocity in 2D graphene. Using the formalism outlined in Sec. II leads to a scattering matrix element,

$$\widetilde{V}_{\mathrm{ac}}(q_y) = D_{\mathrm{ac}}|q_y|(1 + e^{i\theta_{kk'}}) \sqrt{\frac{n^{\pm}\hbar}{8\rho LW\omega}} \delta_{q_y, \Delta k_y}, \qquad (15)$$

where the Kronecker delta function $\delta_{q_y, \Delta k_y}$ ensures the momentum conservation for the carrier + acoustic phonon system, and Δk_y is the change in the wave vector in the scattering event. The resulting intrasubband scattering rate is given by the Fermi golden rule to be

$$\frac{1}{\tau_{\mathrm{ac}}(\mathcal{E})} = \frac{n_{\mathrm{ph}} D_{\mathrm{ac}}^2 \mathcal{E}}{\hbar^2 v_F^2 \rho v_s W}(1 + \cos \theta_{kk'}), \qquad (16)$$

where $n_{\mathrm{ph}} = n^+ + n^-$ is used to take both absorption and emission of acoustic phonons into account. Here $\mathcal{E}$ is the energy of carriers measured with respect to the Dirac point. The scattering rate may be rewritten in the form,

$$\frac{1}{\tau_{\mathrm{ac}}(\mathcal{E})} = \frac{n_{\mathrm{ph}} \pi D_{\mathrm{ac}}^2 q_y^2}{4\rho W\omega_{\mathrm{ac}}} \rho_{\mathrm{GNR}}(\mathcal{E})(1 + \cos \theta_{kk'}), \qquad (17)$$

where backscattering restricts the value of $|q_y| = 2|k_y|$. This form highlights the proportionality of the scattering rate to the DOS of the GNR. The scattering rate is also inversely proportional to the width of the GNR and becomes more severe for narrower ribbons, similar to the diameter dependence in carbon nanotubes.[21]

B. Optical phonons

For optical-phonon scattering, we consider the zone-boundary phonon of energy $\hbar\omega_{\mathrm{LO}} \sim 160$ meV, with an optical deformation potential $D_{\mathrm{op}} \sim 1.4 \times 10^9$ eV/cm, assumed to be the same as for 2D graphene. Optical-phonon scattering is inelastic; at low bias voltages and small electric fields, optical-phonon emission by carriers is energetically forbidden, and absorption is damped by the high energy and low population of LO phonons. Since the emission of optical phonons is possible only if the kinetic energy of carriers exceeds $\hbar\omega_{\mathrm{LO}}$, this mechanism is important only for highly energetic carriers.

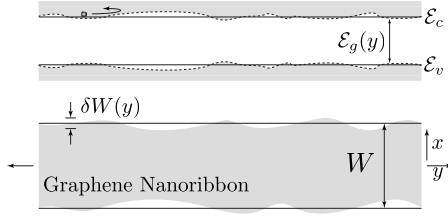The perturbation potential introduced by LO phonons is given by[24]

FIG. 1. Schematic representation of LER scattering in GNRs. The variation in the GNR width leads to spatial variation in the band gap, and the fluctuations in the band edges cause carrier scattering and reduction in mobility.

$$V_{\mathrm{op}}(y) = \sqrt{\frac{n^{\pm}\hbar}{2\rho L W \omega_{\mathrm{LO}}}} D_{\mathrm{op}} e^{i q_y y}, \qquad (18)$$

where $n^- = 1/[\exp(\hbar\omega_{\mathrm{LO}}/k_B T) - 1]$, $n^+ = 1 + n^-$, similar to those of acoustic phonons. The matrix element for optical-phonon scattering is given by

$$\widetilde{V}_{\mathrm{op}}(q_y) = D_{\mathrm{op}}(1 + e^{i\theta_{kk'}}) \sqrt{\frac{n^{\pm}\hbar}{8\rho L W \omega_{\mathrm{LO}}}} \delta_{q_y, \Delta k_y}, \qquad (19)$$

and the final scattering rate is given by

$$\frac{1}{\tau_{\mathrm{op}}(\mathcal{E})} = \frac{n^{\pm}\pi D_{\mathrm{op}}^2}{4\rho W \omega_{\mathrm{LO}}} \rho_{\mathrm{GNR}}(\mathcal{E}')(1 + \cos\theta_{kk'}), \qquad (20)$$

where the energy of the carrier after the scattering event changes to $\mathcal{E}' = \mathcal{E} \pm \hbar\omega_{\mathrm{LO}}$.

C. Line-edge roughness scattering

To capture the effect of line-edge roughness of the GNR on charge transport, the width of ribbon is treated as a function of the longitudinal axis y. The width is given by $W(y) = W + \delta W(y)$, where $\delta W(y)$ describes the roughness and W is the spatially averaged width $[\langle W(y)\rangle = W$, and $\langle \delta W(y)\rangle = 0]$. This is shown schematically in Fig. 1. The edge roughness $\delta W(y)$ can effectively be described by two parameters and by an exponential spatial correlation function,

$$\langle \delta W(y)\delta W(y + \Delta y)\rangle = H^2 e^{-|\Delta y|/\Lambda}, \qquad (21)$$

where H is the amplitude and Λ is the correlation length of the roughness. The LER leads to a spatially modulated band gap and the resulting fluctuations in the band-edge potential cause the scattering of carriers. The perturbation potential for the nth subband is given by

$$V_{\mathrm{LER}}(y) = -\frac{\delta W(y)}{W}\mathcal{E}_n, \qquad (22)$$

where $\mathcal{E}_n = \hbar v_F |k_n|$ is the conduction-band energy of the nth subband relative to the Dirac point.

Since the scattering potential is only dependent on the longitudinal axis, the scattering is intrasubband. The square of matrix element of the nth subband is given by

$$|V_{\mathrm{LER}}(q_y)|^2 = \frac{\mathcal{E}_n^2}{L}\frac{H^2}{W^2}\frac{\Lambda}{1 + (\Delta k_y \Lambda)^2}(1 + \cos\theta_{kk'}), \qquad (23)$$

leading to a scattering rate,

$$\frac{1}{\tau_{\mathrm{LER}}(\mathcal{E})} = \frac{\pi\mathcal{E}_n^2}{\hbar}\frac{H^2}{W^2}\frac{\Lambda}{1 + 4k_y^2\Lambda^2}\rho_{\mathrm{GNR}}(\mathcal{E})(1 + \cos\theta_{kk'}). \qquad (24)$$

Since $\mathcal{E}_n \propto 1/W$, the scattering rate is proportional to $1/W^4$. Moreover if the LER scattering rate is dominant, the mobility should scale with the width of the GNR as $\mu_{\mathrm{LER}} \sim W^4$. This behavior contrasts with interface and/or surface roughness scattering in traditional semiconductors with parabolic band structures. Since energy eigenvalues in such traditional semiconductors are proportional to W^{-2}, confinement of carriers into a length scale of W leads to a roughness scattering limited mobility which scales as $\mu_{\mathrm{IR}} \sim W^6$.[20] Thus, the band structure of GNRs make them *inherently more robust* to LER scattering than parabolic band-gap semiconductor nanostructures of comparable size.

In addition to the W^{-4} dependence of the LER scattering rate, the dependence on the roughness amplitude is $\propto H^2$. The factor $\Lambda/(1 + 4k_y^2\Lambda^2)$ is maximized for $2k_y \sim 1/\Lambda$, indicating that LER scattering is the most severe for those carriers in the GNR that have Fermi wavelengths of the same order as the correlation length of the fluctuations.

The LER scattering rates evaluated for realistic GNRs are plotted in Figs. 2(a) and 2(b). Figure 2(a) shows the LER scattering rate as a function of the roughness amplitude, ranging from $\sim 1\%$ to $\sim 50\%$ of the GNR width, for nominal GNR widths of $W = 3$, 5, 8, and 12 nm. The correlation length for this plot is $\Lambda \sim 3$ nm. Figure 2(b) illustrates the dependence of the scattering rate on the Fermi level; as the Fermi level in the GNR is increased by a gate voltage, the Fermi wavelength of carriers decrease, and therefore, LER scattering becomes more sensitive to roughness at shorter correlation lengths. Therefore, for $2k_y\Lambda \ll 1$ and for $2k_y\Lambda \gg 1$, the LER scattering rate is low.

We note here that for very rough GNR edges characterized by $H \sim W \sim \Lambda$, it is possible that carriers are localized in quantum-dot-like confining potentials; transport in such rough GNRs will occur by hopping and tunneling between localized states as opposed to diffusive band transport (see Ref. 25). The transport treated in this work is restricted to the diffusive band-transport regime.

D. Impurity scattering

Due to an impurity charge located at $(x_0, 0, z)$ with respect to the GNR which is on the $z = 0$ plane (see Fig. 3), the unscreened scattering potential experienced by a mobile electron located at $(x, y, 0)$ in the GNR is given by the Coulomb potential,

$$V_{\mathrm{Coul}}(x_0, y, z) = \frac{e^2}{4\pi\epsilon_0\kappa\sqrt{d^2 + y^2}}, \qquad (25)$$

where z is the distance of the impurity from the GNR plane and κ is average relative dielectric constant of materials on the two sides of the GNR.[26] The distance of the impurity from the origin is $d = \sqrt{z^2 + (x - x_0)^2}$. The *screened* impurity perturbation matrix element is then given by
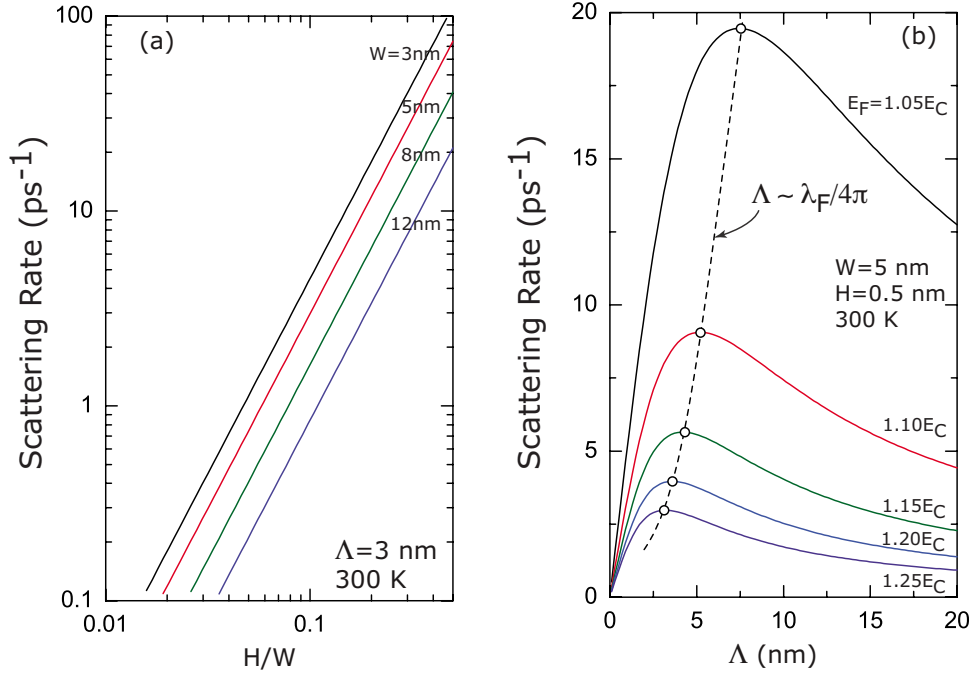
FIG. 2. (Color online) Line-edge roughness scattering rates in GNRs (a) for various GNR widths W plotted against a range of roughness amplitudes (H normalized to the widths W) and (b) for a 5-nm-wide ribbon for various Fermi levels plotted against various roughness correlation lengths Λ.

$$V_{\text{Coul}}(q_y) = (1 + e^{i\theta_{kk'}}) \frac{e^2}{4\pi\epsilon_0\kappa\epsilon_{\text{scr}}} \frac{1}{LW} \int_0^W K_0(|\Delta k_y|d)dx,$$

$$(26)$$

where $\Delta k_y = k_y - k_{y'}$ is the change in the carrier wave vector along the GNR axis upon scattering, $K_0(\ )$ is the zeroth-order modified Bessel function, and ϵ_{scr} is the screening factor in Eq. (13).

In order to get the scattering rate due to all impurities, we integrate over the distribution of impurities. For the most general distribution of impurities, the scattering rate is given by

$$\frac{1}{\tau_{\text{imp}}(\mathcal{E})} = \frac{2\pi}{\hbar}\left(\frac{e^2}{4\pi\epsilon_0\kappa\epsilon_{\text{scr}}W}\right)^2 \rho_{\text{GNR}}(\mathcal{E})\mathcal{S}(k_y, W)$$

$$\times (1 + \cos\theta_{kk'}), \qquad (27)$$

where $\mathcal{S}$ is an effective scattering "cross section" with dimensions of length given by

$$\mathcal{S}(k_y, W) = \int_0^t n_{3D}(z)dz \int_{-\infty}^{\infty} dx_0 \left|\int_0^W K_0(2k_yd)dx\right|^2.$$

$$(28)$$

Here $n_{3D}(z)$ is the volume density of the impurities which can vary with the distance from the GNR plane and t is the thickness over which the impurities are distributed. This general formalism allows us to evaluate, at the same time, the effect of scattering by volume-distributed impurities as well as impurities located at the GNR surface. If the charged impurities are located at the GNR/dielectric interface or on the GNR surface, then the scattering rate is found unambiguously by taking $z \to 0$ and $n_{3D}(z) \to n_{2D}\delta(z)$, where n_{2D} is the 2D impurity density. For the evaluation of the scattering rates in the rest of the paper, we consider the volume (bulk) and surface impurities separately to highlight their relative importance. This is motivated by the recent observation that for 2D graphene, surface impurities are responsible for low-field mobility,[10] and when they are removed, an order of magnitude improvement in mobility is observed even at room temperature.[27,28]

E. Comparison of the scattering rates

The rates for each type of scattering mechanism are first evaluated as a function of carrier energy to gauge their relative importance. They are plotted in Fig. 4 for a GNR of $W=5$ nm width at $T=300$ K. The relevant parameters used for the calculation are an edge roughness characterized by $(H, \Lambda)=(0.5, 3)$ nm, a bulk impurity density $n_{3D}=10^{15}/\text{cm}^3$, and a surface impurity density $n_{2D}=10^{10}/\text{cm}^2$. In addition to the individual scattering rates, the total scattering rate obtained by Matheissens' rule as a sum of the individual scattering rates is also shown. For the specific case of the parameters chosen, the LER scattering is seen to dominate at low
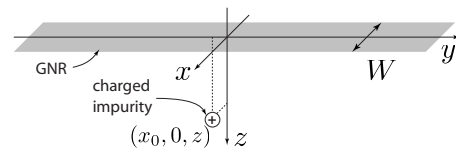

FIG. 3. Schematic representation of the GNR and charged impurities that cause scattering of mobile carriers.
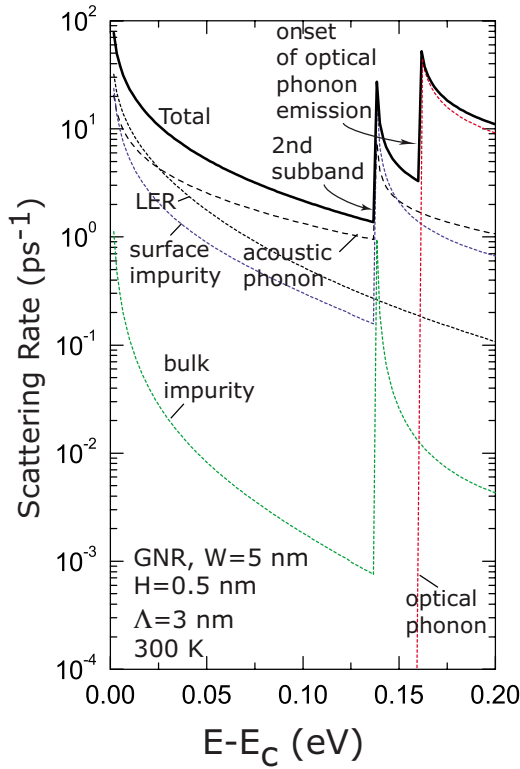
FIG. 4. (Color online) Scattering rates due to various scattering mechanisms for a 5-nm-wide GNR as a function of the carrier energy.

carrier energies, followed by acoustic phonon and surface impurity scattering. The effect of bulk impurities is found to be relatively weak compared to LER and surface impurities. It is possible to experimentally lower (or eliminate) scattering due to LER, bulk, and surface impurities, as they are not *intrinsic* to the GNR, and such techniques are expected to be developed in due course.

The intrinsic scattering mechanisms due to acoustic and optical phonons are also shown in the figure. Due to the dependence of the scattering rates on the 1D DOS of the GNR, the general trend is a decrease in scattering rates as the energy of the state increases from the band edge ($\mathcal{E}_c$) and then the appearance of a step at the onset of the next sub-band. When the energy of a state is $\mathcal{E}_c + \hbar\omega_{LO}$, optical-phonon emission is allowed, and for such high-energy states, optical-phonon scattering dominates over all other scattering mechanisms. This is especially important at high-bias conditions when high-energy states are occupied. Optical-phonon scattering is responsible for the saturation of current flow through the GNR leading to a sharp degradation of carrier mobility. The same has been found earlier for carbon nanotubes.[29] With the evaluation of the various scattering rates, we are in a position to calculate values of low-bias mobilities. The rest of this work discusses low-field mobility in GNRs; high-field and hot carrier effects are not considered here.

IV. CARRIER MOBILITY

Using the formalism for the calculation of carrier mobilities outlined in Sec. II, the carrier mobility is calculated for a 5-nm-wide GNR as a function of temperature for three different locations of the Fermi level. The impurity densities used in this calculation are $n_{3D} = 10^{15}/\text{cm}^3$ and $n_{2D} = 10^{10}/\text{cm}^2$. The results are shown in Fig. 5. Note that $\mathcal{E}_c$ is the conduction-band edge, which is half the band gap above the Dirac point. When the Fermi level is located in the band gap at $\mathcal{E}_F = 0.75\mathcal{E}_c$ from the Dirac point, the carrier mobility is severely affected by surface impurity scattering at low temperatures as seen in Fig. 5(a). Above ~200 K, acoustic-phonon scattering dominates the scattering rate. The dominance of surface impurity scattering for this case is due to the fact that when $\mathcal{E}_F = 0.75\mathcal{E}_c$ and the temperature is low, the net
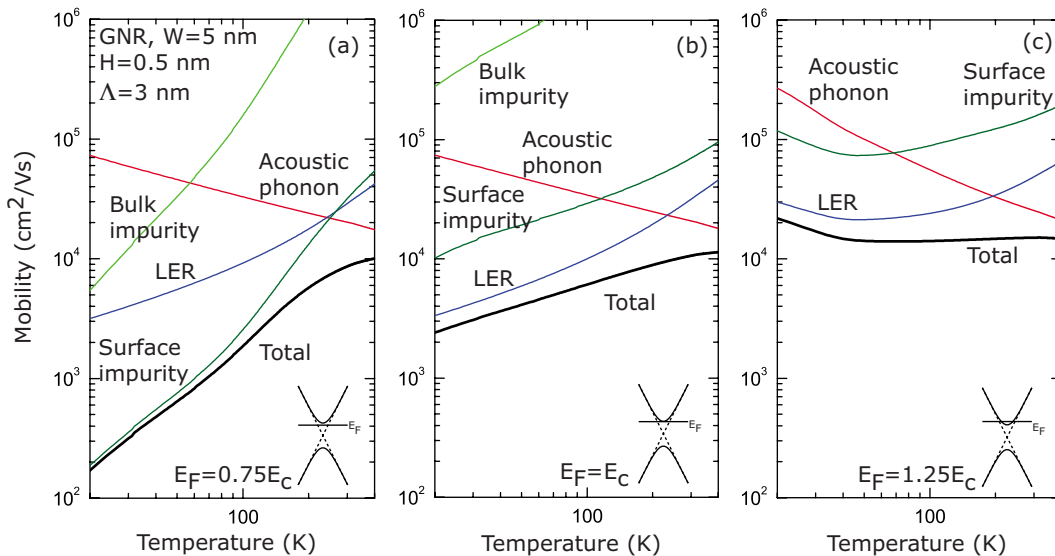

FIG. 5. (Color online) Carrier mobility in a 5 nm GNR as a function of temperature for three distinct Fermi levels. The relative importance of the various scattering rates can be ascertained from the plots. E_c is the energy difference between the conduction-band edge and the Dirac point of the underlying graphene band structure.
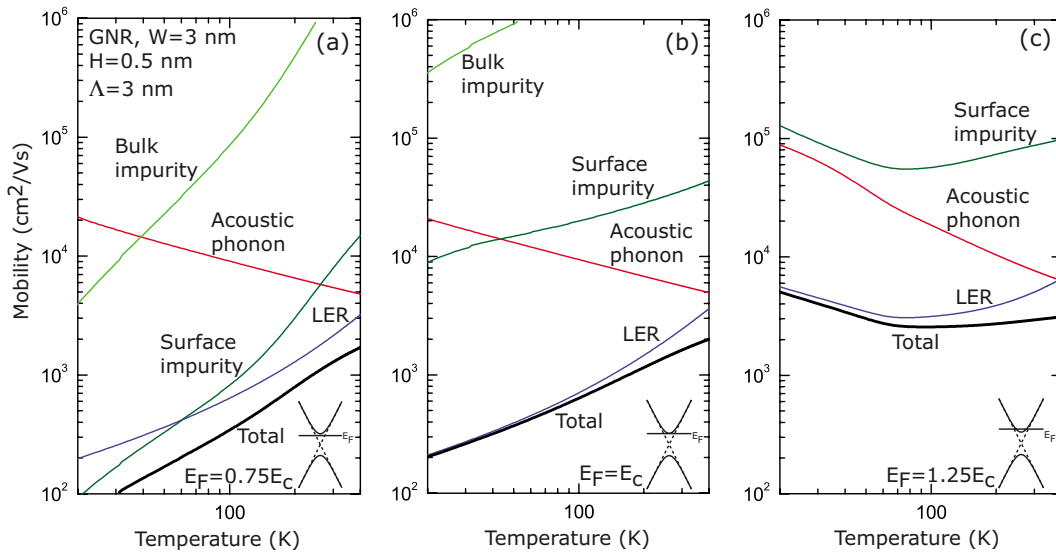
FIG. 6. (Color online) Carrier mobility in a 3 nm GNR as a function of temperature for three distinct Fermi levels.

mobile electron density in the conduction band is low, and screening is weak. As the Fermi level is raised to the conduction-band edge—$\mathcal{E}_F=\mathcal{E}_c$ [Fig. 5(b)]—and then above it—$\mathcal{E}_F=1.25\mathcal{E}_c$ [Fig. 5(c)]—surface Coulomb impurities are strongly screened, and LER scattering dominates at low temperatures. At and around room temperature, acoustic-phonon scattering still limits the electron mobility. The effect of LER scattering is felt only when the surface impurity density is low. The surface impurity scattering rate scales inversely with the density of impurities; thus if the surface impurity density is much higher, say $n_{2D}\sim10^{12}/cm^2$, it becomes the dominant scattering mechanism, limiting the room-temperature mobility to $10–1000$ cm²/V s. Mobilities in this range has been recently reported in ultrathin GNRs.[7] But due to the lack of experimental evidence of the GNR edge roughness of such samples, it is early to make a direct comparison. However, from the analysis, it can be concluded that such values of mobilities are not *intrinsic* and result from either LER or surface impurity scattering.

If the width of the GNR is lowered to $W=3$ nm but with a roughness the same as the 5-nm-wide GNR, LER scattering becomes stronger. Figure 6 depicts the relative importance of the various scattering mechanisms at different temperature for three locations of the Fermi level. As can be seen, LER scattering starts dominating at and around room temperature as well, overtaking acoustic-phonon scattering. If one considers the case when surface and bulk impurities are absent, the mobility will be determined by the relative importance of acoustic phonon and LER scattering.

Finally, if the surface impurity density is lowered to a level $\ll10^{10}/cm^2$, the LER and acoustic-phonon scattering mechanisms are of the most interest. Under such a condition, the mobility is plotted as a function of the GNR width for a constant edge roughness in Fig. 7. The crossover of the LER and acoustic-phonon scattering rates occurs at $W\sim4$ nm for the chosen edge roughness parameters. For narrow ribbons, LER scattering dominates, but as the width of the GNR is increased, the LER scattering rate decreases as W^4, making

the GNRs of widths 5 nm and above relatively insensitive to edge roughness scattering. As $W\rightarrow\infty$, the acoustic-phonon scattering rate limit on the mobility approaches that of 2D graphene; indeed, mobilities as high as $120,000$ cm²/V s have been recently observed in suspended 2D graphene sheets when the surface impurities were removed by current-induced annealing.[27]
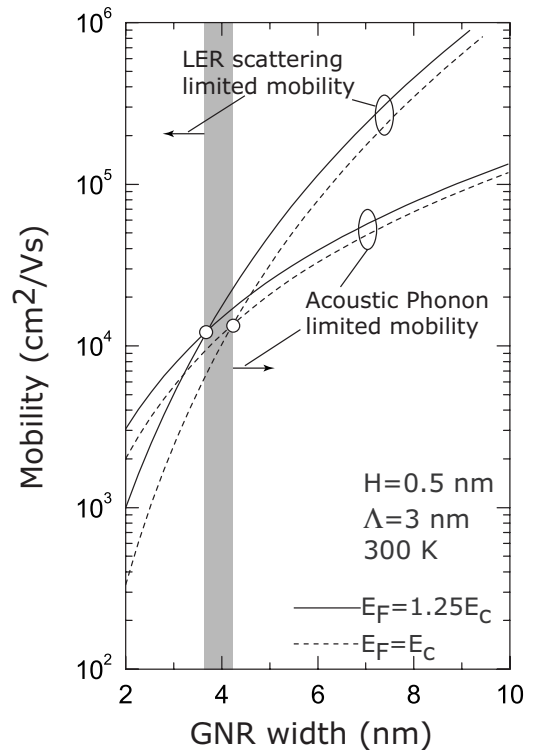

FIG. 7. For very narrow ribbons, LER scattering is seen to be the mobility-limiting scattering mechanism but wider GNRs—even for widths greater than ~5 nm are relatively insensitive to LER scattering. For such ribbons, the mobility at room temperature is limited by acoustic-phonon scattering.

V. CONCLUSIONS

In conclusion, it is shown from analytical modeling that low-field carrier transport in GNRs is affected by intrinsic scattering by acoustic phonons, in addition to line-edge roughness and impurity scattering. Impurities sticking to the GNR surface or at the interface of GNRs and underlying substrates are much more deleterious than those embedded in the underlying substrate. For very thin GNRs, the mobility is degraded by LER scattering, which reduces the mobility as the fourth power of the GNR width. For many technologically relevant GNR widths, LER scattering is weaker than the intrinsic acoustic-phonon scattering.

*djena@nd.edu

[1] A. Geim and K. S. Novoselov, Nature Mater. **6**, 183 (2007).

[2] K. S. Novoselov, A. K. Geim, S. V. Morozov, D. Jiang, M. I. Katsnelson, I. V. Grigorieva, S. V. Dubonos, and A. A. Firsov, Nature (London) **438**, 197 (2005).

[3] C. Berger, Z. Song, X. Li, X. Wu, N. Brown, C. Naud, D. Mayou, T. Li, J. Hass, A. Marchenkov, E. Conrad, P. First, and W. A. de Heer, Science **312**, 1191 (2006).

[4] M. Y. Han, B. Ozyilmaz, Y. Zhang, and P. Kim, Phys. Rev. Lett. **98**, 206805 (2007).

[5] X. Li, X. Wang, L. Zhang, S. Lee, and H. Dai, Science **319**, 1229 (2008).

[6] G. Fiori and G. Iannaccone, IEEE Electron Device Lett. **28**, 760 (2007).

[7] X. Wang, Y. Ouyang, X. Li, H. Wang, J. Guo, and H. Dai, Phys. Rev. Lett. **100**, 206803 (2008).

[8] S. V. Morozov, K. S. Novoselov, M. I. Katsnelson, F. Schedin, D. C. Elias, J. A. Jaszczak, and A. K. Geim, Phys. Rev. Lett. **100**, 016602 (2008).

[9] T. Ando, J. Phys. Soc. Jpn. **75**, 074716 (2006).

[10] J. H. Chen, C. Jang, S. Adam, M. S. Fuhrer, E. D. Williams, and M. Ishigami, Nat. Phys. **4**, 377 (2008).

[11] H. M. Dong, W. Xu, Z. Zeng, T. C. Lu, and F. M. Peeters, Phys. Rev. B **77**, 235402 (2008).

[12] N. M. R. Peres, J. M. B. Lopes dos Santos, and T. Stauber, Phys. Rev. B **76**, 073412 (2007); also see T. Stauber, N. M. R. Peres, and F. Guinea, *ibid.* **76**, 205423 (2007).

[13] V. V. Cheianov and V. I. Fal'ko, Phys. Rev. Lett. **97**, 226801 (2006).

[14] E. H. Hwang and S. Das Sarma, Phys. Rev. B **75**, 205418 (2007).

[15] K. Seeger, *Semiconductor Physics: An Introduction*, 7th ed. (Springer-Verlag, Berlin, 1999), p. 50.

[16] B. Trauzettel, D. V. Bulaev, D. Loss, and G. Burkard, Nat. Phys. **3**, 192 (2007).

[17] L. Brey and H. A. Fertig, Phys. Rev. B **73**, 235411 (2006).

[18] L. Brey and H. A. Fertig, Phys. Rev. B **75**, 125434 (2007).

[19] K. Hirakawa and H. Sakaki, Phys. Rev. B **33**, 8291 (1986).

[20] H. Sakaki, T. Noda, K. Hirakawa, M. Tanaka, and T. Matsusue, Appl. Phys. Lett. **51**, 1934 (1987).

[21] B. Obradovic, R. Kotlyar, F. Heinz, P. Matagne, T. Rakshit, M. D. Giles, M. A. Stettler, and D. E. Nikonov, Appl. Phys. Lett. **88**, 142102 (2006).

[22] K. Seeger, *Semiconductor Physics: An Introduction*, 7th ed. (Springer-Verlag, Berlin, 1999), p. 175.

[23] G. Pennington, A. Goldsman, A. Akturk, and A. E. Wickenden, Appl. Phys. Lett. **90**, 062110 (2007).

[24] K. Seeger, *Semiconductor Physics: An Introduction*, 7th ed. (Springer-Verlag, Berlin, 1999), p. 204.

[25] F. Sols, F. Guinea, and A. H. Castro Neto, Phys. Rev. Lett. **99**, 166803 (2007).

[26] Fringing fields are neglected here due to the 1D geometry of the GNR. This approximation does not have a major impact on the dominant scattering rate determination since bulk impurity scattering is found to be weaker than the surface impurity.

[27] K. I. Bolotin, K. J. Sikes, J. Hone, H. L. Stormer, and P. Kim, Phys. Rev. Lett. **101**, 096802 (2008).

[28] S. Adam and S. DasSarma, Solid State Commun. **146**, 356 (2008).

[29] V. Perebeinos, J. Tersoff, and P. Avouris, Phys. Rev. Lett. **94**, 086802 (2005).